Theor Chem Acc (2006) 115: 391–397
DOI 10.1007/s00214-005-0073-1

REGULAR ARTICLE

Ling Zhang · J. Ilja Siepmann

Direct calculation of Henry's law constants from Gibbs ensemble Monte Carlo simulations: nitrogen, oxygen, carbon dioxide and methane in ethanol

Received: 9 September 2005 / Accepted: 12 December 2005 / Published online: 17 January 2006
© Springer-Verlag 2006

Abstract Configurational-bias Monte Carlo simulations in the Gibbs ensemble were used to calculate Henry's law constants, Ostwald solubilities, and Gibbs free energies of transfer for oxygen, nitrogen, methane, and carbon dioxide in ethanol at 323 and 373 K. These three solubility descriptors can be expressed as functions of mechanical properties that are directly observable in the Gibbs ensemble approach, thereby allowing for very precise determination of the descriptors. Additionally, the Henry's law constants of multiple solutes can be computed from a single simulation. Most of the simulations were carried out for systems containing 1,000 solvent and up to 8 solute molecules, and further simulations using either 500 or 2,000 solvent molecules point to negligible system size effects. A comparison with experimental data shows that the united-atom version of the transferable potential for phase equilibria force field yields Henry's law constants that reproduce well the differences between the four solutes and the changes upon increase of the temperature.

1 Introduction

The Henry's law constant, $H_{2,1}(T, p)$, of a solute 2 (gas) in a solvent 1 (liquid) is an important descriptor for the solubility of a volatile compound at a given temperature, T and pressure, p, and it is defined as the limiting ratio at infinite dilution of the equilibrium partial pressure of the solute in the gas phase, p_{gas}, to its concentration in the (liquid) solution, x_2 [1,2]

$$H_{2,1}(T, p) = \lim_{x_2 \to 0} p_2^{\text{gas}} / x_2^{\text{liq}}. \tag{1}$$

L. Zhang · J.I. Siepmann (✉)
Departments of Chemistry and of Chemical Engineering and Materials Science,
University of Minnesota,
207 Pleasant Street SE,
Minneapolis, MN 55455-0431,
USA
E-mail: siepmann@chem.umn.edu

Thus the value of the Henry's law constant depends on the type of solute, the solvent, and the temperature while the pressure is usually taken as the saturated vapor pressure for this binary system (but could also be an elevated pressure due to the presence of other volatile components). Unfortunately, different units are often used for the Henry's law constant depending on the chosen units for the partial pressure and the solute concentration. In this work, the former is given in terms of megaPascals, while dimensionless mole fraction is used for the concentration.

Experimental difficulties in high-temperature measurements of Henry's law constants arise for many technologically important mixtures when the solvent is flammable and/or the solute is an oxidizing agent, e.g., solubility of oxygen in ethanol. Thus, computational methods that can accurately predict Henry's law constant are highly desirable.

Different approaches have been used to compute Henry's law constants from particle-based simulations. However, the equilibrium partial pressure of the solute in the gas phase, p_2^{gas} in Eq. (1), is not an observable property in conventional simulations of closed systems, and as suggested by Shing et al. [3] the Henry's law constant is usually determined by its relationship to the excess chemical potential

$$H_{2,1}(T, p) = \lim_{x_2 \to 0} k_{\text{B}} T \rho_1(T, p) \exp\left[\frac{\mu_2^{\text{ex}}(T, p, x_2)}{k_{\text{B}} T}\right], \tag{2}$$

where k_{B}, ρ_1, and μ_2^{ex} are Boltzmann's constant, the density of the (neat) solvent, and the excess chemical potential of the solute, respectively. The use of Eq. (2) requires prior knowledge of the density of the (neat) solvent and its saturated vapor pressure for the force field used in the simulation (because the experimental values might not be reproduced by this force field) before the excess chemical potential can be computed.

The most popular simulation approaches to determine μ_2^{ex} are based on the concept of free energy perturbation [4, 5] that involves a perturbation of a reference system (usually

the neat solvent) to a different system (usually containing one additional solute particle). For example, Widom's ghost particle insertion method [6,7] relates $\mu_2^{ex}(T, V)$ via the ratio of the canonical ensemble partition functions (for systems with N solvent particles and with N solvent + 1 solute particles) to the ensemble-averaged potential energy experienced by a 'ghost' solute particle in a system of N solvent molecules. A similar relationship accounting for volume fluctuations also exists for μ_2^{ex} in the isobaric–isothermal ensemble [8]. Unfortunately, as has been recently demonstrated by Kofke and Cummings [9,10], the application of free energy perturbation methods can result in systematic errors depending on the phase–space relationship between the reference and perturbed systems.

Another popular technique to determine free energy differences, such as μ_2^{ex}, is the expanded ensemble approach [11] that uses a collection of sub-ensembles (either in the canonical or the isobaric–isothermal ensemble) to cover the range from the reference system to the target system. The chemical potential can be computed from the probabilities with which the reference and target systems are visited. However, an efficient computation requires biasing the simulation trajectory so that these end states and all intermediate states are frequently sampled, which is usually achieved through iterative adjustment of the biasing factors. Recently, Cichowski et al. [12] have proposed a self-adaptive transition matrix Monte Carlo (TMMC) method that alleviates this iterative process and allows for the efficient computation of Henry's law constants.

In this work, it is demonstrated that simulations in the Gibbs ensemble [13–15] can be used to directly compute Henry's law constants in a way analogous to experiments, i.e., a two-phase system is used to directly obtain the saturated vapor pressure and the solute mole fractions in the vapor and liquid phases. The Gibbs ensemble approach has previously been used to compute Gibbs free energies of transfer for volatile and relatively involatile compounds [16–19]. Beyond great statistical precision, this Gibbs ensemble route offers three significant advantages: (1) sophisticated configurational-bias Monte Carlo (CBMC) particle insertion/deletion moves [20,21] that use only part of the intermolecular potential for the calculation of Rosenbluth weights [22] can be employed, whereas these time saving split-energy techniques are not permissible for computations of residual chemical potentials [20]; (2) since the Gibbs ensemble simulation automatically finds the correct saturated vapor pressure and the solvent density, there is no need to compute these properties of the solvent separately before carrying out a calculation for the Henry's law constant; and (3) following the lead of experimental work, the Gibbs ensemble technique can also be used to compute Henry's law constants of multiple solutes from a single simulation. The same Gibbs ensemble simulations also provide data for the Ostwald solubility from the ratio of the number densities of the solute in the liquid and gas phases. Extensive comparisons are is made with experimental data and recent computations by Cichowski et al. [12] using the TMMC approach.

2 Simulation Details

A combination of the *NVT* version of the Gibbs ensemble Monte Carlo (GEMC) method [13] and the coupled–decoupled CBMC algorithm [23] was used to calculate Henry's law constants for CO_2, CH_4, N_2, and O_2 in ethanol at two different temperatures (323 and 373 K) and the corresponding saturated vapor pressure. These GEMC simulations utilize two separate simulation boxes for the vapor and liquid phases. Both solvent and solute molecules are allowed to swap between the two simulation boxes to equilibrate their chemical potentials between the two phases, and the volume can be exchanged from one box to the other to reach mechanical equilibrium.

The frequency of the particle swap moves was adjusted so that a swap move is accepted about once every ten Monte Carlo (MC) cycles (one cycle consists of N MC moves with N being the total number of molecules in the system). To enhance the acceptance rate for particle swap moves, the CBMC algorithm together with multiple insertions for the first bead [24,25] and a split-energy approach [20,21] were applied. The latter approach employs a shorter-range potential truncation (R_{inner}) for the Lennard–Jones (LJ) interactions and the direct-space part of the Ewald sum for Coulombic interactions during the computation of the Rosenbluth weight for the multiple trial sites, which is then corrected only for the selected trial conformation in the CBMC acceptance step [20, 21]. This split-energy approach results in a significant increase of computational efficiency in particular for systems with long-range Coulombic interactions.

The frequency of the volume moves was also adjusted to yield about one accepted volume move per ten MC cycles. The total volume of the two simulation boxes was set to a value that satisfies the condition that on average approximately half of the total number of solute molecules can be found in the vapor box and half in the liquid box.

The remainder of the MC moves is distributed evenly over the conventional degrees of freedom for the solvent and solute molecules, which are translations, rotations around the center of mass, and conformational changes for ethanol.

The majority of the simulations used a system size with 1,000 solvent molecules (initially all placed in the liquid box) and a small number of solute molecules of a given type (initially all placed in the vapor box). To investigate the concentration dependence of the Henry's law constant, simulations were carried out with 1, 2, 4, or 8 solute molecules. With the exception of one set of simulations containing four different solute types, separate simulations were conducted for each type of solute at each temperature. The simulations for the 1,000-solvent systems were equilibrated for at least 50,000 MC cycles, followed by production runs consisting of at least 300,000 cycles. The statistical uncertainties reported in this study are standard errors of the mean obtained from carrying out four independent simulations for each system (solute type/solute concentration/temperature).

To compute the Henry's law constant, x_2^{liq} in Eq. (1) can be taken directly from the ensemble average of this property,

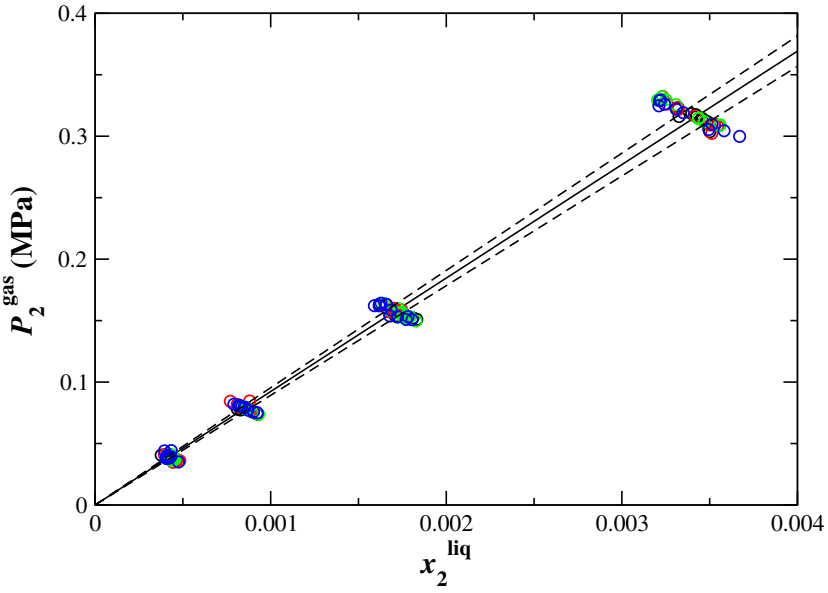

Fig. 1 Partial pressure versus liquid-phase mole fraction for methane in ethanol. The simulation data for blocks of 30,000 MC cycles are depicted by *circles*, and the *different colors* denote block data from the four independent simulations. The *solid* and *dashed lines* are the corresponding weighted linear fit and its standard error of the mean

and p_2^{gas} is computed using Dalton's law of partial pressures from the ensemble averaged mole fraction of the solute in the gas phase, x_2^{gas}, and the ensemble averaged saturation pressure, p_{sat}.

3 Force field

The united-atom version of the transferable potentials for phase equilibria (TraPPE–UA) [21,26,27] force field was used to model the ethanol solvent. The TraPPE–UA force field utilizes pseudo-atoms located at the carbon positions to represent entire methyl or methylene groups, thereby reducing the number of interaction sites and computer time needed to simulate the system. The nonbonded part of the TraPPE force field consists of pairwise additive LJ and Coulombic interactions. Fixed partial charges are used to model the first-order electrostatic interactions of the alcohol head group by placing charges at the polar hydrogen, oxygen, and α-carbon atoms. This solvent model yields excellent agreement for the saturated liquid density and vapor pressure of neat ethanol [26].

Simulations for methane were carried out using both its united-atom and explicit-hydrogen representations of the TraPPE force field [21,28], and rigid three-site models [29] were used for carbon dioxide (three LJ and three partial-charge sites) and nitrogen (two LJ and three partial-charge sites). For this work, a rigid three-site model for oxygen was parameterized by fitting to the vapor–liquid coexistence curve of neat oxygen ($d_{\text{OO}} = 1.21$ Å; $\sigma_{\text{O}}(\text{O}_2) = 3.02$ Å; $\epsilon_{\text{O}}(\text{O}_2)/k_{\text{B}} = 49$ K; $q_{\text{O}}(\text{O}_2) = -0.113e$ with a compensating counter-charge of $+0.226e$ at the bond center).

For LJ interactions, the standard Lorentz–Berthelot combining rules were used for unlike pairs [30] and a site–site based spherical potential truncation at 14 Å was employed together with analytical tail corrections for the energy and pressure [30,31]. Electrostatic interactions were computed using the Ewald summation technique with tin-foil boundary conditions [30].

It should be noted here that Cichowski et al. [12] also used the TraPPE–UA force field for their TMMC simulations and that, with the exception of the oxygen parameters (see above), the force-field parameters are the same in the TMMC and GEMC studies.

4 Results and discussion

4.1 Henry's law constants

Figure 1 shows a plot of the partial pressure of methane (TraPPE–EH representation) versus its liquid-phase mole fraction in the ethanol solvent at 323 K (and the corresponding saturated vapor pressure). The four groups of data represent the simulation results for the systems with a different number of solute molecules (ranging from 1 to 8). For each system, the data are shown separately for blocks of 30,000 MC cycles (ten blocks for each run). Although there is some spread in the data for the individual blocks, they cluster together nicely around a mean value. Most importantly, it appears that the results for all four concentrations can be well described by a linear fit (i.e., the concentrations are sufficiently low that deviations from the Henry's law are not significant compared to the statistical uncertainties of the simulations). Similar graphs were

Table 1 Henry's law constants in megaPascals (mole fraction basis)

Solute	T [K]	GEMC	TMMC	Experiment
N_2	323	220.5 ± 4.8	217 ± 8	253.6 ± 7.6
	373	191.0 ± 5.3	193 ± 3	221.3 ± 13.3
O_2	323	125.6 ± 2.9	125 ± 3	174.8 ± 8.7
	373	123.6 ± 2.8	125 ± 3	159.9 ± 12.8
CH_4(UA)	323	87.1 ± 2.1	86 ± 2	81.5 ± 2.4
	373	91.9 ± 2.4	94 ± 2	83.4 ± 5.0
CH_4(EH)	323	92.3 ± 3.1		81.5 ± 2.4
	373	104.6 ± 2.9		83.4 ± 5.0
CO_2	323	17.2 ± 0.4	17.8 ± 0.6	21.1 ± 1.1
	373	27.1 ± 0.5	28.0 ± 0.4	29.7 ± 3.3

Comparison of the GEMC (this work) and TMMC [12] simulation data and of the experimental benchmark data [32]. The statistical uncertainties given for the simulation data are standard errors of the mean (GEMC) and standard deviations (TMMC) computed from four independent simulations

obtained for the TraPPE–UA representation of methane and for the other three solutes (nitrogen, oxygen, carbon dioxide).

To determine the Henry's law constant, the averages for x_2^{liq} and p_2^{gas} are first computed, followed by a weighted linear fit constrained to pass through the origin. The numerical data for the Henry's law constants obtained from the GEMC simulations are listed in Table 1 and compared to the TMMC data by Cichowski et al. [12] and the experimental benchmark data by Friend et al. [32]. By definition, a larger Henry's law constant signals a lower gas solubility. For both temperatures, the Henry's law constants in ethanol fall into the order nitrogen > oxygen > methane > carbon dioxide (and for the solubilities: carbon dioxide > methane > oxygen > nitrogen). That is, the gas solubilities increase in the same order as the critical temperatures of the neat gases (CO_2: 304 K; CH_4: 190 K; O_2: 154 K; N_2: 128 K). Both the GEMC and TMMC simulation studies reproduce the experimental data very well with mean unsigned percentage errors of 15% for both GEMC (with UA methane) and TMMC. (Here, it should be noted that a different oxygen model without quadrupole moment was used in the TMMC simulations [12].) The GEMC simulations also show that using the explicit-hydrogen representation for methane yields predictions for the Henry's law constant in (united-atom) ethanol that are not as good as those for the united-atom version. Thus, it appears that some caution should be applied when using the different versions (united-atom and explicit-hydrogen representations of alkyl segments) of the TraPPE force field together.

Overall, it appears that the simulations underpredict Henry's law constants (overpredict the solubility) for the three quadrupolar solutes (N_2, O_2, CO_2), whereas the opposite is true for the nonpolar CH_4 solute. Nevertheless, the TMMC and GEMC data for O_2 are in very good agreement despite the former using an oxygen model without explicit partial charges [33]; a model with three explicit partial charges is used here. A similar observation was also made by Cichowski et al. [12] who compared nitrogen models with and without partial charges. Thus, it appears that one might focus on the ethanol solvent model when one wants to further improve the accuracy of the predicted Henry's law constants for the solute/solvent combinations studied here. However, the 15% mean unsigned percentage error in the Henry's law constant corresponds to an error of only 0.4 kJ/mol in the Gibbs free energy of transfer, a rather small error compared to other predictive methods.

The uncertainties in the experimental benchmark data are about 6% and arise from the precision of the experiments, extrapolation of the data to infinite dilution (while $x_2^{\text{liq}} \approx 0.02$ were used for N_2, CH_4, and CO_2), and correction of the data to the reference pressure (while the experiments were carried out at pressures ranging from 0.4 to 7 MPa) [32]. Remarkably, both GEMC and TMMC simulations yield statistical uncertainties that are smaller than the experimental uncertainties. The experimental uncertainties are larger at the higher temperature but they decrease with increasing temperature for the simulations because phase space is sampled better at higher temperatures. It appears that there is no significant difference in the statistical uncertainties obtained for the GEMC and TMMC simulations after accounting for the different run lengths (about 900,000 MC cycles for TMMC vs. 300,000 cycles for GEMC).

Figure 2 shows a comparison of the Henry's law constants calculated from the GEMC simulations with the experimental benchmark data [32] and additional experimental data: nitrogen [34–37], oxygen [36], methane [34,36,38], and carbon dioxide [34]. Due to the scarcity of direct experimental data for the Henry's law constants of these systems, the plot also includes values which were derived from experimental data for the dilute region of the vapor–liquid coexistence curves for the binary mixtures of CH_4/ethanol [38–40] and CO_2/ethanol [39] and from experimental data for the Ostwald solubility coefficients, $L_{2,1}(T, p)$, of nitrogen and oxygen [41]. The Ostwald solubility and Henry's law constant are related via [2]

$$L_{2,1}(T, p) = \frac{C_2^{\text{liq}}}{C_2^{\text{gas}}} \simeq \frac{RT\rho^{\text{liq}}}{H_{2,1} M_{\text{w},1}}, \tag{3}$$

where C_2^{liq} and C_2^{gas} are the molar concentrations (or number densities) for solute 2 in the liquid and gas phase, respectively; ρ^{liq} and $M_{\text{w},1}$ are the specific density of the neat solvent and its molecular mass, respectively; and R is the molar gas constant.

The changes following increase in temperature from 323 to 373 K for Henry's law constants of the four solutes calculated from the GEMC and TMMC simulations are the same within the statistical uncertainties and the simulation data for the TraPPE–UA model are in excellent agreement with experiments, i.e., all predicted temperature ratios lie within the uncertainties of the experimental benchmark data (see Table 2 and Fig. 2). The data for the EH representation of methane differ somewhat more, but still fall within the combined uncertainties of experiment and GEMC simulation.

As the temperature is raised from 323 to 373 K, a decrease in the Henry's law constant of about 15% is observed for nitrogen, whereas that for carbon dioxide increases by about

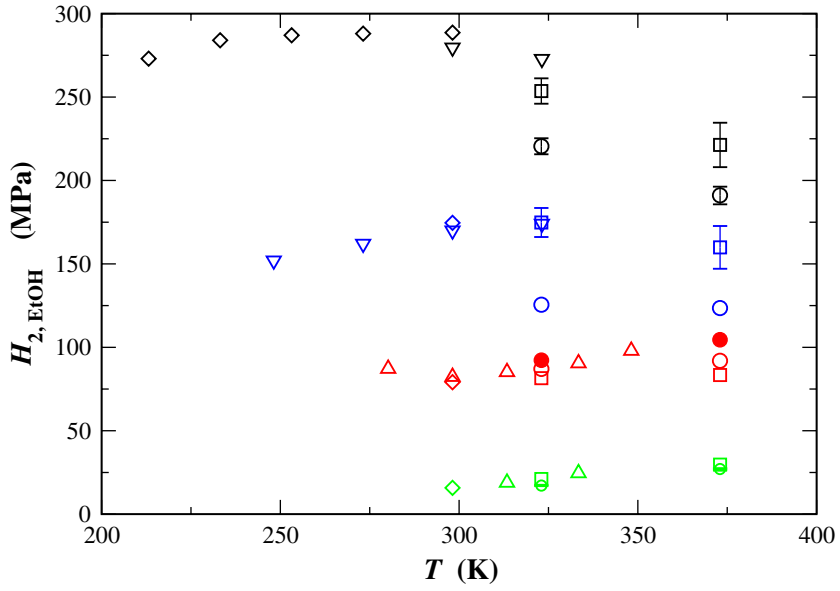

Fig. 2 Temperature dependence of the Henry's law constants (mole fraction basis) for N_2 (*black*), O_2 (*blue*), CH_4 (*red*), and CO_2 (*green*) in ethanol. The experimental benchmark data [32] and GEMC simulation data are depicted by *squares* and *circles* (*filled circles* for EH representation of methane), respectively (*error bars* are only shown when larger than symbol size). Other experimental data for direct measurements of the Henry's law constant [34–37], converted from binary vapor–liquid coexistence curves [39,40] or from the Ostwald solubilities [41] are shown as *diamonds*, *up-triangles*, and *down-triangles*, respectively

Table 2 Ratio of Henry's law constants, $H_{2,1}(323\ \mathrm{K}, p)/H_{2,1}(373\ \mathrm{K}, p)$ for the GEMC simulations and for the experimental benchmark data [32]

Solute	GEMC	Experiment
N_2	1.15 ± 0.04	1.15 ± 0.08
O_2	1.02 ± 0.03	1.09 ± 0.10
CH_4(UA)	0.95 ± 0.03	0.98 ± 0.06
CH_4(EH)	0.88 ± 0.04	0.98 ± 0.06
CO_2	0.64 ± 0.02	0.71 ± 0.09

30%. The increase for methane is smaller with GEMC values of 5 and 12% for the UA and EH representations, respectively. The benchmark data for methane yield an increase of only 2%, but values derived from binary vapor–liquid coexistence curves [39,40] show a somewhat larger increase. The benchmark data for oxygen [32] show a decrease of 9%, whereas GEMC and TMMC yield essentially the same values for both temperatures and earlier experimental data [41] even point to an increase for temperatures below 323 K.

The origin of the different trends in solubility caused by the change in temperature for the four solutes is not obvious. At least for the temperature range studied here, it appears that the solubilities for the more soluble solutes (CO_2 and CH_4) decrease, whereas that for the least soluble solute (N_2) increases. Furthermore, additional experimental data point to a solubility minimum for nitrogen [35–37] and oxygen [32, 41] and to a maximum for methane [40,36,39]. A decrease in solubility is often viewed as driven by the entropic penalty of solvation, but the heat capacity of transfer may play an equally important role [42].

4.2 System size effects

Particle-based simulations are always carried out for system sizes far from the thermodynamic limit, and it is, therefore, important to assess the system-size dependence of the calculated properties. This is particularly important here because the calculation of excess chemical potentials is known to depend on system size [17,43]. To test whether the standard system size containing 1,000 solvent molecules used here is appropriate, additional GEMC simulations were carried out at 323 and 373 K for CO_2/ethanol systems containing 500 solvent and 1 solute molecules and 2,000 solvent and 4 solute molecules, i.e., changing the system size but keeping the overall composition constant. For comparison, the TMMC simulations were carried out for systems containing 216 ethanol molecules and 1 solute molecule. The production periods for the 500 and 2,000 solvent molecule systems consisted of 300,000 and 200,000 MC cycles, respectively.

Henry's law constants, Ostwald solubilities, and free energies of transfer calculated for the three different system sizes are in excellent agreement (see Table 3), i.e., systems containing a few hundred solvent molecules appear to be sufficient for a reliable calculation of Henry's law constants in the Gibbs ensemble. A similar conclusion was previously reached for the determination of Gibbs free energies of transfer from GEMC simulations [17]. It should be noted here that the Henry's law constants listed in Tables 1 and 3 are not exactly the same because the latter were computed using only one overall composition, while four different compositions were used for the former.

Table 3 System size dependence of the Henry's law constant (mole fraction basis), Ostwald solubility, and Gibbs free energy of transfer for carbon dioxide in ethanol obtained from GEMC simulations using only one solute concentration

T [K]	System size	$H_{2,1}$ [MPa]	$L_{2,1}$	ΔG_{trans} [kJ/mol]
323	500:1	18.0 ± 0.5	2.44 ± 0.03	-2.40 ± 0.03
	1000:2	17.7 ± 0.6	2.48 ± 0.03	-2.44 ± 0.03
	2000:4	18.0 ± 0.8	2.45 ± 0.08	-2.41 ± 0.09
373	500:1	27.2 ± 0.7	1.64 ± 0.03	-1.53 ± 0.06
	1000:2	26.5 ± 0.7	1.68 ± 0.03	-1.61 ± 0.06
	2000:4	27.2 ± 0.8	1.64 ± 0.06	-1.53 ± 0.11

Table 4 Comparison of Henry's law constants in megaPascals (mole fraction basis) obtained from standard and concurrent simulations

T [K]	Solute	Standard	Concurrent
323	N_2	220.5 ± 4.8	222.9 ± 3.7
	O_2	125.6 ± 2.9	128.4 ± 1.7
	CH_4	87.1 ± 2.1	86.0 ± 1.5
	CO_2	17.2 ± 0.4	17.9 ± 0.5
373	N_2	191.0 ± 5.3	190.2 ± 2.6
	O_2	123.6 ± 2.8	124.1 ± 1.6
	CH_4	91.9 ± 2.4	89.9 ± 1.4
	CO_2	27.1 ± 0.5	27.7 ± 0.5

4.3 Concurrent determination of Henry's law constants for multiple solutes

Given the observation that a relatively small system size yields accurate results for the Henry's law constant of a single solute type, it also needs to be checked whether the solubilities of multiple solutes can be determined from a single GEMC simulation. Similarly, experimental measurements are often carried out concurrently for multiple solutes. For example, the benchmark experiments [32] used dilute mixtures of oxygen and nitrogen (for obvious safety reasons). Furthermore, it should be mentioned that Widom's ghost particle insertion method [6,7] can also be applied to multiple solutes with only a negligible overhead because the same set of solvent configurations can be used in each case. An extension of the expanded ensemble approach to multiple solutes would be somewhat more involved because additional subensembles would be required.

For the standard GEMC protocol described in Sect. 2, simulations were carried out separately for four different solutes and four different compositions (and using four independent runs), i.e., a total of 16 solute type/concentration combinations using 1,000 solvent molecules. If it would be possible to reduce this to a single simulation containing concurrently all four solutes and still obtain reasonable results, then the benefit of GEMC simulation over traditional free-energy perturbation methods would be even more profound.

The concurrent simulation systems used here contained only 500 solvent molecules and 1 molecule for each solute type (504 molecules in total) and were run for 600,000 MC cycles (twice as long as the standard simulations) at both temperatures. Again, four independent simulations were used to estimate the standard error of the mean.

It should be noted that the overall simulation volume for the standard simulations was adjusted during the equilibration period to allow for about equal numbers of solute molecules in the gas and liquid phases. This is, of course, not possible for multiple solutes (where the volume can only be adjusted to yield roughly equal numbers for the sum of the four solutes in the two phases) which will increase the statistical uncertainties for the solutes with the largest and the smallest Henry's law constants.

Table 4 shows a comparison of the Henry's law constants obtained from the concurrent and standard GEMC simulations. As can be seen, the data for the concurrent and standard simulations agree within their combined uncertainties for all four solutes and two temperatures. However, given that the concurrent simulations required a factor of about 25 less computer time (4 independent runs of 600,000 MC cycles for 500 solvent molecules versus 64 runs of 300,000 cycles for 1,000 solvent molecules), the results for the concurrent simulations are very encouraging and this approach appears to be best when Henry's law data for multiple solutes needs to be computed.

5 Conclusions

This study shows that configurational-bias MC simulations in the Gibbs ensemble allow the precise determination of Henry's law constants, Ostwald solubilities (or partition coefficients), and Gibbs free energies of transfer. The Gibbs ensemble data shows excellent agreement with recent predictions obtained using a transition matrix MC approach [12]. The predicted data for the TraPPE–UA force field yield a mean unsigned error of 15% from experimental benchmark data [32] and the temperature dependence of the Henry's law constants is very well reproduced. The largest deviations are observed for the solubility of oxygen, whereas the deviations for nitrogen, methane, and carbon dioxide are somewhat smaller. It should be noted here that binary vapor–liquid equilibria with alkanes were exploited in the force field development to obtain an improved balance of the LJ and Coulombic interactions in the nitrogen and carbon dioxide models [29].

Computations of the Henry's law constants for different system sizes demonstrate that 500 solvent molecules are sufficient to yield reliable predictions. More importantly, it is also shown that the Henry's law constants of multiple solutes can be calculated concurrently from a single simulation in the Gibbs ensemble.

Although they are not required for the solute/solvent combinations studied here, it should be mentioned that use of special balancing factors [44] allows for an extension of the Gibbs ensemble approach to the calculations of Gibbs free energies of transfer for cases where the gas solubilities are either very low or very high (leading to large uncertainties in x_2^{liq} or p_2^{gas}, respectively). These balancing factors are preset external potentials acting on a specific solute type in a specific phase, which are very similar in spirit to the biasing

parameter used in expanded-ensemble simulations [11] and, which can be removed in the calculation of the Gibbs free energy of transfer [44]. However, even with these balancing factors, the Gibbs ensemble acceptance rate for complete particle swaps might become prohibitively low and either an expanded Gibbs ensemble approach [45] or a family of homologous solutes [16,44] need to be used.

Acknowledgements We thank Marcus Martin for stimulating discussions and Jeffrey Errington for providing a preprint of Ref. [12]. Financial support from the National Science Foundation (CTS-0138393) is gratefully acknowledged. Part of the computer resources were provided by the Minnesota Supercomputing Institute.

References

1. Prausnitz JM, Lichtenthaler RN, Azevedo EGD (1986) Molecular thermodynamics of fluid phase equilibria. Prentice Hall, Englewood Cliffs
2. Sandler SI (1989) Chemical and engineering thermodynamics. Wiley, New York
3. Shing KS, Gubbins KE, Lucas K (1988) Mol Phys 65:1235
4. Jorgensen WL (1989) Acc Chem Res 22:184
5. Kollman PA (1996) Acc Chem Res 29:461
6. Widom B (1963) J Chem Phys 39:2808
7. Widom B (1982) J Phys Chem 86:869
8. Sindzingre P, Ciccotti G, Massobrio C, Frenkel D (1987) Chem Phys Lett 136:35
9. Kofke DA, Cummings PT (1997) Mol Phys 92:973
10. Kofke DA (2004) Mol Phys 102:405
11. Lyubartsev AP, Martsinovski AA, Shevkunov SV, Vorontsov-Velyaminov PN (1992) J Chem Phys 96:1776
12. Cichowski EC, Schmidt TR, Errington JR (2005) Fluid Phase Equil 236:58
13. Panagiotopoulos AZ (1987) Mol Phys 61:813
14. Panagiotopoulos AZ, Quirke N, Stapleton M, Tildesley DJ (1988) Mol Phys 63:527
15. Smit B, de Smedt P, Frenkel D (1989) Mol Phys 68:931
16. Martin MG, Siepmann JI (1997) J Am Chem Soc 119:8921
17. Martin MG, Siepmann JI (1998) Theo Chem Acc 99:347
18. Chen B, Siepmann JI (2000) J Am Chem Soc 122:6464
19. Wick CD, Siepmann JI, Schure MR (2004) Anal Chem 76:2886
20. Vlugt TJH, Martin MG, Smit B, Siepmann JI, Krishna R (1998) Mol Phys 94:727
21. Martin MG, Siepmann JI (1998) J Phys Chem B 102:2569
22. Siepmann JI, Frenkel D (1992) Mol Phys 75:59
23. Martin MG, Siepmann JI (1999) J Phys Chem B 103:4508
24. Esselink K, Loyens LDJC, Smit B (1995) Phys Rev E 51:1560
25. Mackie AD, Tavitian B, Boutin A, Fuchs AH (1997) Mol Simul 19:1
26. Chen B, Potoff JJ, Siepmann JI (2001) J Phys Chem B 105:3093
27. http://www.chem.umn.edu/groups/siepmann/trappe/intro.php
28. Chen B, Siepmann JI (1999) J Phys Chem B 103:5370
29. Potoff JJ, Siepmann JI (2001) AIChE J 47:1676
30. Allen MP, Tildesley DJ (1987) Computer simulation of liquids. Oxford University Press, Oxford
31. Wood WW, Parker FR (1957) J Chem Phys 27:720
32. Friend DG, Frurip DJ, Lemmon EW, Morrison RE, Olson JD, Wilson LC (2005) Fluid Phase Equil 236:15
33. Coon JE, Gupta S, McLaughlin E (1987) Chem Phys 113:43
34. Wilhelm E, Battino R (1973) Chem Rev 73:1
35. Katayama T, Nitta T (1976) J Chem Eng Data 21:194
36. Bo S, Battino R, Wilhelm E (1993) J Chem Eng Data 38:611
37. Fischer K, Wilken M (2001) J Chem Thermodyn 33:1285
38. Ukai T, Kodama D, Miyazaki J, Kato M (2002) J Chem Eng Data 47:1320
39. Suzuki K, Sue H, Itou M, Smith RL, Inomata H, Arai K, Saito S (1990) J Chem Eng Data 35:63
40. Brunner E, Hultenschmidt W (1990) J Chem Thermodyn 22:73
41. Kretschmer CB, Nowakowska J, Wiebe R (1946) Ind Eng Chem 38:506
42. Wick CD, Siepmann JI, Schure MR (2003) J Phys Chem B 107:10623
43. Siepmann JI, McDonald IR, Frenkel D (1992) J Phys Condens Matter 4:679
44. Chen B, Siepmann JI (2005) J Phys Chem B, ASAP article
45. Escobedo FA, de Pablo JJ (1996) J Chem Phys 105:4391